Article

Analysis of Crop Reflectance for Estimating Biomass in Rice Canopies at Different Phenological Stages

Martin Leon Gnyp, Kang Yu, Helge Aasen, Cologne, Yinkun Yao, Shanyu Huang, Yuxin Miao, Beijing, China & Georg Bareth, Cologne

Summary: This paper contributes an assessment for estimating rice (*Oryza sativa L., irrigated lowland rice*) biomass by canopy reflectance in the Sanjiang Plain, China. Hyperspectral data were captured with field spectroradiometers in experimental field plots and farmers' fields and then accompanied by destructive aboveground biomass (AGB) sampling at different phenological growth stages. Best single bands, best two band-combinations, optimised simple ratio (SR), and optimised normalized ratio index (NRI), as well as multiple linear regression (MLR) were calculated from the reflectance for the non-destructive estimation of rice AGB. Experimental field data were used as the calibration dataset and farmers' field data as the validation dataset. Reflectance analyses display several sensitive bands correlated to rice AGB, e.g. 550, 670, 708, 936, 1125, and 1670 nm, which changed depending on the phenological growth stages. These bands were detected by correlograms for SR, NRI, and MLR with an offset of approximately ± 10 nm. The assessment of the three methods showed clear advantages of MLR over SR and NRI in estimating rice AGB at the tillering and stem elongation stages by fitting and evaluating the models. The optimal band number for MLR was set to four to avoid overfitting. The best validated MLR model ($R^2 = 0.82$) at the tillering stage was using four bands at 672, 696, 814 and 707 nm. Overall, the optimized SR, NRI, and MLR have a great potential in non-destructive estimation of rice AGB at different phenological stages. The performance against the validation dataset showed R^2 of 0.69 for SR and R^2 of 0.70 for NRI, respectively.

Zusammenfassung: *Reflexionsanalyse zur Abschätzung der Biomasse von Reis in unterschiedlichen phänologischen Stadien.* Dieser Beitrag versucht eine Bewertung zur Biomassenabschätzung von Kulturreis (Oryza sativa L., bewässerter Flachland-Kulturreis) mit Hilfe von Bestandsreflexion in der Sanjiang Ebene, China. Hyperspektrale Daten wurden in Freilandexperimenten und in Feldern von Landwirten mit Feldspektroradiometern gemessen. Nach den Spektralmessungen wurde die oberirdische Biomasse destruktiv in unterschiedlichen phänologischen Wachstumsstadien gemessen. Beste einzelne Bänder, beste Zweibandkombinationen, optimierter Simple Ratio (SR) und Normalisierter Ratio Index (NRI), sowie Multiple Regressionsanalyse (MLR) wurden anhand von Reflexionsdaten der Freilandexperimente berechnet. Die Daten von den Feldern der Landwirte wurden als Validierungsdatensatz verwendet. Die Reflexionsanalysen zeigen mehrere zur Biomasse korrelierend sensitive Bänder, z. B. 550 nm, 670 nm, 708 nm, 936 nm, 1125 nm und 1670 nm, welche sich in Abhängigkeit von phänologischen Wachstumsstadien änderten. Diese Bänder wurden mittels Korrelogramme für SR, NRI und MLR mit einem Versatz von ca. ± 10 nm detektiert. Die Bewertung der drei Methoden zeigte deutliche Vorteile von MLR gegenüber SR und NRI in der Biomassenabschätzung für Reis im Bestockungs- und Ährenschwellenstadium. Die optimale Bandanzahl für MLR wurde auf vier festgesetzt, um eine Überanpassung zu vermeiden. Das beste MLR-Modell ($R^2 = 0.82$) zum Bestockungsstadium basiert auf vier Bändern (672 nm, 696 nm, 814 nm und 707 nm). Die Analyse von hyperspektralen Reflexionsdaten zur Optimierung von VIs oder MLR hat ein großes Potential in der Biomassenabschätzung für Reis in unterschiedlichen phänologischen Stadien. Dies wird durch die gute Übertragbarkeit ($R^2 = 0.69$ für SR und $R^2 = 0.70$ für NRI) der optimierten Modelle in die landwirtschaftliche Praxis unterstrichen.

1   Introduction

In the field of crop science, the aboveground dry biomass (AGB) and nutrient use efficiency are considered to be the major factors for determining the final yield (Raun & Johnson 1999). AGB influences at each phenological stage the amount of grain production, since the yield is defined as the amount of grain, straw, and AGB. Furthermore, knowledge of crop development characteristics and its spatial and temporal variation in the field are useful for determining crop requirements such as N-fertilisation as closely as possible and for achieving acceptable yields, e.g. for rice (Fagiera 2007).

Traditional methods to estimate AGB involve direct destructive measurements in the field, which are time-consuming, expensive, and require intensive field work. In the context of precision agriculture, proximal sensing is a promising and well investigated tool to avoid the destructive approach (Gebbers & Adamchuk 2010). Field canopy reflectance can be measured with portable handheld or mobile spectroradiometer, e.g. Yara N-Sensor (AGRICON 2013) and can be used to support farmer's decisions on crop management such as fertilisation, pest management, or irrigation.

Hyperspectral measurements in the field can also be used as groundtruth or for model development in analysing satellite imagery. The disadvantage of hyperspectral and multispectral satellite images is the high dependence on a clear sky at the image aquisition time, while spectroradiometers can be used in the field with some cloud cover for approximately 3–4 hours around solar noon. Spectroradiometers are fast and the most important non-destructive devices. They have a continuous acquisition of all reflectance values in a given spectral range of 350 nm – 2500 nm with a high spectral resolution of < 2 nm – 5 nm (Milton et al. 2009, Ortenberg 2011).

In many studies, the in-field reflectance measurements are acquired and required for calibrating satellite-borne hyperspectral data using, e.g. EO-1 Hyperion imagery (Psomas et al. 2011, Koppe et al. 2012) or of airborne-based data, e.g. HyMap imagery (Cho & Skidmore 2009). The goal of these studies is to es-

timate AGB on a large scale using airborne or satellite-borne remote sensing data by applying evaluated models. The hyperspectral satellite EnMap, which is scheduled for 2016, will provide data with two separate sensors for the aquisition of VNIR and SWIR in the spectral domain of 420 nm – 2450 nm with 30 m ground resolution similar to the Hyperion data (Schwind et al. 2012). By simulating the spectral properties of EnMap with field spectroradiometer data, models can be developed and evaluated for EnMap-based estimation of AGB (Kaufmann et al. 2010).

The relationship between reflectance and agricultural crop characteristics has been investigated in many studies in the last decades (Thenkabail et al. 2000). Most of those studies focused on nitrogen, leaf area index (LAI), or yield estimation, but rarely on AGB estimation, since there is a strong correlation between LAI and AGB (Shibayama & Akiyama 1989, Fillela & Penuelas 1994). Studies that use hyperspectral ground data to estimate AGB have been carried out for grass, wheat, and for rice (Richardson et al. 1983, Shibayama & Akiyama 1986, Anderson & Hanson 1992, Serrano et al. 2000, Hansen & Schjoerring 2003, Li et al. 2010, Wang et al. 2008, Bajwa et al. 2010).

The common method to estimate AGB from reflectance is based on the application, improvement, or development of spectral indices (SIs). Optimised or improved standard SIs such as SR and NRI represent best band selections based on correlograms (Thenkabail et al. 2000, Stroppiana et al. 2009, Koppe et al. 2010). In addition, MLR has been applied in several studies, since this method provides flexibility in the choice of bands (Shibayama & Akiyama 1989, Takahashi et al. 2000, Yu et al. 2013). Futhermore, MLR is more reliable than SIs that is saturated at high LAI levels (Yang & Chen 2004, Haboudane et al. 2004). It is simpler and more flexible for the adoption by growers and crop consultants than partial least square (PLS) (Bajwa et al. 2010).

Many AGB studies were conducted in greenhouses under controlled conditions or the spectral reflectance was measured in the laboratory (Song et al. 2011), but not in the field. Furthermore, most results, proposed SIs, or developed models were not validated us-

ing an independent dataset to test the transferability of the models. Previous studies have often focused only on calibrating wavebands to a crop parameter, and have not adequately evaluated the performance of their results in an independent dataset (Lu 2006, Cho & Skidmore 2009).

The main two objectives of this study are (i) to investigate the potential for rice AGB estimation from the canopy reflectance and (ii) to develop and evaluate the proposed AGB estimation models. The first step contains an analysis of the AGB variation, the analysis of the relationship between canopy reflectance and N-application and AGB. In a second step, three methods to estimate AGB by the reflectance are tested with a calibration dataset using experimental field data: Single bands, best two band-combinations (SR and NRI), and MLR. Finally, the three methods are transferred to an independent dataset using farmers' field data under conventional management.

2 Material and Methods

2.1 Study Area and Experimental Design

The research was carried out at the Qixing farm (47.2 °N, 132.8 °E) in Jiansanjiang, Heilongjiang Province, Northeast China. The farm is located in the Sanjiang Plain (Fig. 1), which is an alluvial plain from three rivers (Heilongjiang, Songhua, Wusuli), and covers about 109,000 km^2. The area is characterised by a sub-humid continental monsoon climate. The mean annual temperature is about 2 °C and the mean precipitation sums up to 550 mm per year. The frost-free period is about 130 days long. The rice fields belong to the northernmost cropping rice system in China and to the northernmost ones worldwide. The rice is sown in mid-April (in heated greenhouses), is transplanted after the frost period to the field from the middle to the end of May, and is harvested around end of September. The fields are controlled flooded and manured with N-fertiliser before transplanting the seedlings. Four to five seedlings (120–150 seedlings/m^2) are planted at one position forming a so-called hill. The irrigation is usually stopped 30 days before harvest.

Two field experiments were carried out at two sites (Keyansuo and Qixing research station) in Jiansanjiang and were used as the calibration dataset. They represented a wide range of growth conditions by N-fertiliser input conducted in a split-plot design: 0, 60, 75, 90, 105, 120, and 150 kg N ha^{-1} in 2007 (146 plots), and 0, 35, 70, 105, and 140 kg N ha^{-1} in 2008 (88 plots) and 2009 (95 plots). The plot size was approximately 20 m^2 each. The widely used rice variety *Kongyu131* (28 hills/m^2) was cultivated in all experiments. In addition to the experimental fields, 9 farmers' fields were selected in 2007–2009 and used as the validation dataset. They were managed by the farmers according to their usual practices. The size of these fields varied from 12 to 27 ha, where each field contained several plots with a mean
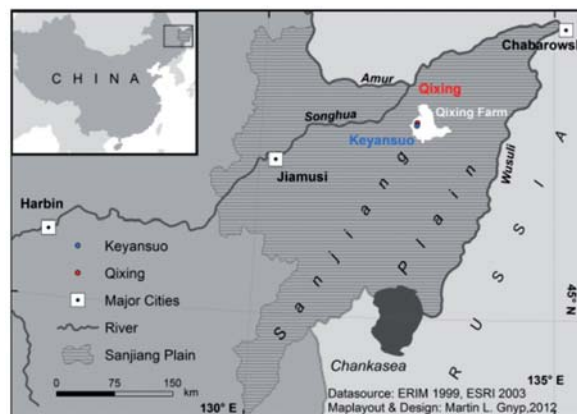

Fig. 1: Study area in the north-east corner of China.

size of 1,400 m². In most cases, the cultivar *Kongyu131* was planted.

2.2 Hyperspectral Data Collection

Hyperspectral and agronomic data were collected in 2007–2009. Before taking the spectral reflectance, the average number of tillers in each hill was determined per plot in order to measure the reflectance of representative plants (Fig. 2). Canopy spectral reflectance was measured with two non-imaging passive sensors by ASD (Analytical Spectral Devices, Inc., Boulder, CO, USA): QualitySpec® Pro in the wavelength domain of 350 nm – 1800 nm in 2007 and 2009, and FieldSpec3® Pro in the wavelength domain of 350 nm – 2500 nm in 2008. Both devices have a sampling interval of 1.4 nm in the VNIR and 2 nm in the SWIR domain. The measurements were taken from 9 a.m. to 1 p.m. LMT, mostly under cloudfree conditions in the field. Every 10 to 15 minutes, calibration measurements were taken with a white reference panel (BaSO$_4$) and were repeated depending on illumination changes. A default viewing angle (α) of 25° and a measuring height (h) of 1 m above the canopy created a field of view (A) of 0.15 m² with a radius (r) of 22 cm (1) and (2).

$$r(m) = h \times tan(\alpha \mid 2) \tag{1}$$

$$A(m^2) = \pi \times r^2 \tag{2}$$

Fig. 2: Hyperspectral data collection in paddy rice (distance to canopy: 0.3 m).

Ten sample counts in the spectrum averaging (settings in the ASD software) were repeated at 6 positions per plot. They were averaged per plot in order to reduce the atmospheric influence, e.g. clouds and wind, and field conditions, e.g. planting in rows. Overall, approximately 14,000 spectra (unaveraged) were collected from 2007 to 2009.

2.3 Aboveground Biomass (AGB) Collection

The AGB was measured destructively by clipping three (booting to heading stage) to five (tillering to stem elongation stage) hills of the measured rice plants. All plant samples were rinsed with water, the roots were clipped, and then the samples were divided in their plant organs leaf, stem and head. They were oven dried at 105 °C for 30 minutes, and dried at 70 °C until constant weight. The AGB was weighed later. In this study, the combined total dry AGB was used and not the individual AGBs from the different organs (leaf, stem, head). Altogether, 1,685 AGB samples were collected from the tillering to heading stages.

2.4 Spectral Indices (SIs) and Stepwise Multiple Linear Regression (MLR)

Single bands or combinations of up to four different bands were tested for their explanatory value. In addition, spectral indices representing two bands were analysed: simple ratio (SR) and normalised difference vegetation index (NDVI). They are widely used for the prediction of biophysical quantities of crops and were developed by Jordan (1969) and Rouse et al. (1974). In this study, the focus is on using the best band-combinations to optimise the SR and NDVI for AGB estimation due to the saturation of the NDVI (Haboudane et al. 2004). The optimised NDVI is also known as normalised ratio index (NRI) and was suggested to determine the best band-combinations (Thenkabail et al. 2000, Sims & Gamon 2002). All possible combinations were computed from the wavelengths in the domain of 350 nm – 1800 nm. The two band-combi-

nations were calculated with a self-developed Java program, analysed and plotted as a contour diagram using MATLAB 7.0 software (MATLAB 2013). Due to the noises caused by water absorption in the SWIR domain, the bands from 1330 nm to 1480 nm, and 1770 nm to 1800 nm were excluded from the analyses. Only the best two band-combinations are presented in the results. The SR and NRI equations are defined as (3) and (4):

$$SR = \frac{\rho_1}{\rho_2}; \text{ where } \rho_1 > \rho_2 \qquad (3)$$

$$NRI = \frac{\rho_1 - \rho_2}{\rho_1 + \rho_2}; \text{ where } \rho_1 > \rho_2 \qquad (4)$$

where
ρ reflectance value

For the analysis of AGB in relation to one feature, irrespectively if a single band or index was used, correlation analysis was applied. The method attempts to model the relationship between two or more variables by fitting a linear regression equation to observed data. Single bands, but also combination of two, three, and four different bands were tested using a stepwise multiple linear regression (MLR). This allows selecting predictors of dependent variable based on statistical criteria. The observed data is the dependent variable of the model. In this study, the AGB is the dependent variable and the single bands are the independent variables. In total, 1,250 bands were analysed in SPSS 20.0 (SPSS 2013) and the best MLR models are presented in the results. The MLR equation is defined as (5):

$$y = a + b_1 \times \rho_{b_1} + b_2 \times \rho_{b_2} + \ldots + b_i \times \rho_{b_i} \qquad (5)$$

where
y	multiple linear regression (MLR)
a	mathematical constant
$b_1, b_2, \ldots, b_i$	coefficients
$\rho_{b1}, \rho_{b2}, \ldots, \rho_{bi}$	reflectances

2.5 *Data Analysis and Statistics*

Original spectral data were used to average the six spectra per plot. The spectra were not smoothed, but significant outliers were excluded from the analysis. In addition, the stepwise MLR provided a method of feature reduction and a statement about the optimal band number to estimate AGB. Basic analyses were conducted like descriptive statistics of AGB, analyses of canopy spectra under different N-rates, and growth stages before using the data as a calibration dataset. The calibrated models were validated using an independent dataset to test the transferability of the models. The following statistic parameters, root-mean-square error (RMSE) and relative error (RE) against the observed mean, were used to calculate the fitness between the observed and estimated data. All statistical analyses were conducted in SPSS 20.0 and Statistica 6.0 (STATISTICA 2013).

3   Results

3.1 *Temporal AGB Variation*

AGB production and development are dependent on crop growth conditions such as weather, soil and nutrition. Tab. 1 illustrates the temporal AGB variation in diverse years and growth stages for the experimental sites. Generally, AGB production tends to increase from the tillering to the heading stage. Overall, it ranges from 0.1 t/ha to 14.1 t/ha across all stages and years. The rice crop had a high variation in AGB (CV > 30 %), especially during the early growth stages. During the later stages booting and heading, the variation was lower (CV < 30 %). Temporal variation between the three years is significant. In 2009, the temperature was lower than in the previous years, so the AGB production was lower with a mean AGB value of 0.8 t/ha – 7.0 t/ha. Highest values were observed in 2008.

Tab. 1: Descriptive statistics of AGB on the experimental fields.

	Stage	n	Min (t/ha)	Max (t/ha)	Mean (t/ha)	SD (t/ha)	CV (%)
2007	Tillering	146	0.1	2.0	0.9	0.46	46.5
	Stem Elongation	74	1.6	5.7	3.4	0.88	26.1
	Booting	49	2.9	7.5	5.6	1.05	18.8
	Heading	114	3.3	12.4	7.6	1.96	26.1
2008	Tillering	40	0.1	1.8	0.9	0.46	50.5
	Stem Elongation	40	0.9	2.9	1.6	0.49	31.3
	Booting	88	2.9	8.8	5.3	1.36	25.6
	Heading	88	4.4	14.1	9.0	1.83	20.4
2009	Tillering	91	0.2	1.6	0.8	0.34	41.3
	Stem Elongation	95	0.3	2.2	1.2	0.52	42.0
	Booting	95	1.4	6.6	3.5	1.26	36.1
	Heading	95	4.6	9.7	7.0	1.15	16.5
All	Tillering	277	0.1	2.0	0.9	0.43	46.3
	Stem Elongation	209	0.3	5.7	2.1	1.19	58.0
	Booting	232	1.4	8.8	4.7	1.57	34.0
	Heading	297	3.3	14.1	7.8	1.87	24.1

n = Number of samples, SD= Standard deviation, CV= Coefficient of variation

3.2 Canopy Reflectance Spectra under Different N-rates and at Different Growth Stages

The reflectance spectra of the rice canopies clearly indicated differences in AGB or LAI that resulted from different N-rates and at various phenological growth stages. The spectra of the experiment plots with five different N-rates at the booting stage in 2008 were taken as an example to display the response pattern of canopy reflectance (Fig. 3, left). Generally, the reflectance spectra tended to increase with rising LAI in the NIR (700 nm – 1100 nm) and SWIR (1100 nm – 1800 nm) regions, whereas the opposite occurred in the VIS (500 nm – 700 nm) region. The canopy LAI responded to N-application. Higher reflectance response occurred with lower N-application. Especially, in the green (500 nm – 600 nm) and red (600 nm – 700 nm) regions, obvious visible differences were detected. There was a high increase in the five spectra in the RedEdge region (670 nm – 740 nm), which were clustered here as one spectrum. Mostly, the differences between the first (0 kg·N/ha) and the second N-rate (35 kg·N/ha) were not significant in the reflectance. Similarities were also observed for the fourth (105 kg·N/ha) and fifth (140 kg·N/ha) N-rate.

Rice canopies showed a diverse reflectance at different growth stages. As an example, a dataset of four stages in 2008 was used to display the response of a rice crop from the tillering to the heading stage (Fig. 3, right). At an early phenological stage, the reflectance was mainly influenced by the soil and water of the paddy field, where the AGB production was low due to low LAI.

Generally, the reflectance increased from the tillering to the booting stage and decreased from the heading stage due to starting senescence of the plant. Maximum reflectance was observed at the booting stage. The canopy LAI and the biochemical components of the plant changed at different growth stages, which evidently influenced the reflectance.
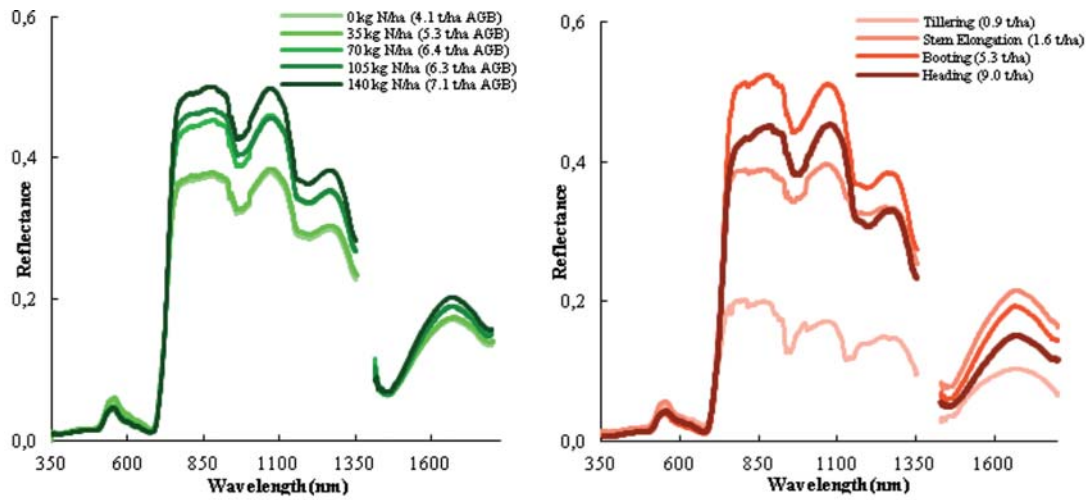
Fig. 3: Left: changes of rice canopy reflectance with varied N-rates at the booting stage in 2008, right: changes in reflectance at different growth stages in 2008.
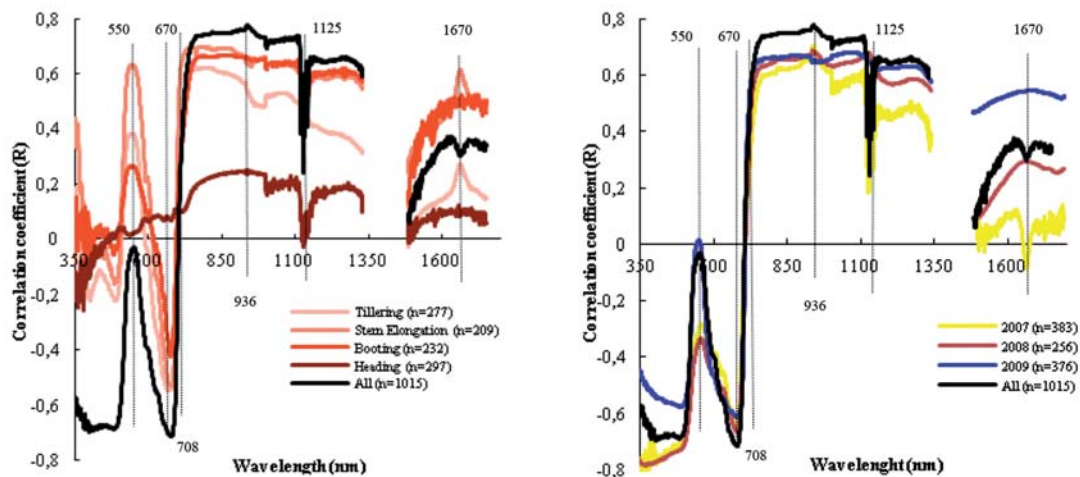

Fig. 4: Left: the correlation coefficients (R) between AGB and canopy reflectance at different phenological stages, right: in different years.

3.3 *Relationship between AGB and Spectral Reflectance*

The correlation coefficients between AGB and canopy reflectance at different phenological stages and in different years are presented in Fig. 4. First of all, the correlation between AGB and reflectance at different stages is described (Fig. 4, left). The pattern of the R (correlation coefficient) curves was similar at the different stages and across all stages except for the heading stage. Lowest absolute R values were observed at the tillering stage as a result of low crop development at this growth stage. Highest R values were recorded at the stem elongation stage and across all stages. Maximum negative R values were observed at tillering and across all stages at wavelengths of 670 nm, which corresponds to high solar radiation absorption by chlorophyll pigments. In the RedEdge region, a high increase of R values was detected, which is coincident with reflectance increase of vegetation in this domain.

Greatest positive R values were observed in the NIR shoulder at the stem elongation

stage and at wavelengths of 936 nm across all stages. Two peaks are noticeable in the SWIR domain. The first one is located as a local minimum in the reflectance at wavelengths of 1125 nm at the booting and heading stages, which is not detected in the early stages of tillering and stem elongation. Additionally, the plotted R curves show some noises in the SWIR domain for the booting and heading stage. The noises were only observed in the 2007 data due to partly cloudy sky during the measurements. As a second peak, a local maximum in the R curves is observed at wavelengths of 1670 nm at tillering and stem elongation.

The plotted curves for the correlation coefficients (R) between AGB and canopy reflectance show strong differences from year to year (Fig. 4, right). In general, the relationship seems to be diverse in all three years. Across all years, the highest R values are observed (R > 0.75), and in 2007 the lowest (R > 0.6). In summary, sensitive bands are located at around 550, 670, 708, 936, 1125 and 1670 nm.

3.4 Model Calibration by single Bands, SR and NRI

The coefficient of determination between AGB and single bands, best SR, and best NRI was calculated. The best single bands and two band-combinations are shown in Tab. 2 at each growth stage and across all three years. Generally, the best SR and NRI always produce higher R^2 values as one single band. SR and NRI show a very similar performance in
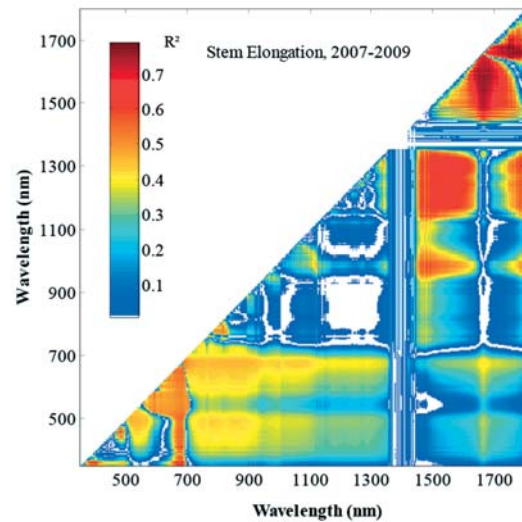

Fig. 5: Best two band-combinations for NRI at the stem elongation stage.

R^2 values except at the stem elongation stage. Moreover, they are similar in the band-combinations ± 20 nm). At the tillering stage, the SR (ρ_{822}, ρ_{716}) has the best performance ($R^2 = 0.58$). At the stem elongation stage, the NRI (ρ_{1678}, ρ_{1575}) displayed the best results ($R^2 = 0.75$) versus other stages (Tab. 2, Fig. 5). At the booting stage, SR (ρ_{695}, ρ_{513}) and NRI (ρ_{695}, ρ_{515}) performed similarly ($R^2 = 0.54$) using almost equal bands. Due to the changes in the canopy reflectance by biochemical components of the plant, all AGB predictors result in lower R^2 values (< 0.3) at the heading stage.

However, across the whole monitored season, high R^2 values were observed ($R^2 > 0.6$) for a high sample number (n = 1015). SR (ρ_{713},

Tab. 2: Single bands, SR and NRI model calibration at different growth stages (2007–2009 pooled data).

Stages (2007–2009)	n	Single Band ρ_1		SR ρ_1/ρ_2		NRI $(\rho_1-\rho_2)/(\rho_1+\rho_2)$	
		ρ_1	R^2	ρ_1, ρ_2	R^2	ρ_1, ρ_2	R^2
Tillering	277	672	0.344	822,716	**0.582**	799,711	0.559
Stem Elongation	209	780	0.487	1760,1325	0.528	1678,1575	**0.758**
Booting	232	854	0.443	695,513	**0.541**	695,515	**0.541**
Heading	297	380	0.066	800,789	0.218	800,789	**0.293**
All	1015	936	0.629	713,550	**0.757**	713,533	0.743

ρ_{550}) showed its best performance here (R^2 = 0.75). The best single band was 936 nm (R^2 = 0.62), which is also important for the MLR models.

3.5 *MLR Model Calibration*

MLR analyses were conducted in two directions: i) assessment of the optimal band number, ii) MLR-models with 1–4 single bands. Generally, with respect to the first direction, the MLR models explain 50–93 % of the variation in AGB (Fig. 6). The highest performance was observed at the stem elongation stage (R^2 = 0.93 with 18 bands), the lowest at the heading stage (R^2 = 0.50 with 17 bands). At the tillering stage, the R^2 reached a value of 0.82 with 19 bands and at the booting stage, a value of 0.60 with 7 bands. The accuracy of the MLR models was quite good. Across all stages, 35 bands explained 88 % of the bio-
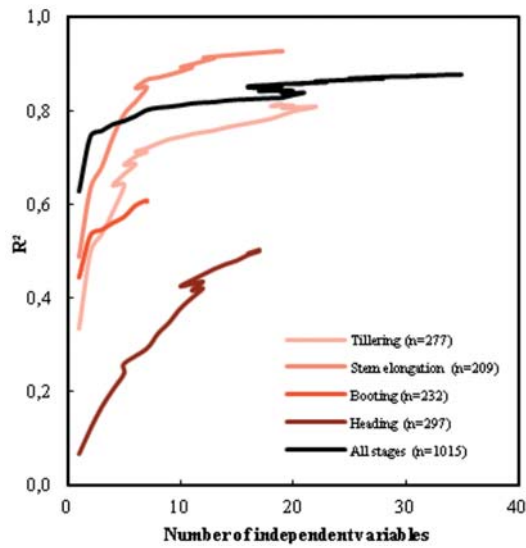

Fig. 6: Relationship between band number and performance (R^2) of the MLR models.

Tab. 3: Stepwise MLR models at diverse growth stages (MLR = multiple linear regression, adj. = adjusted, SE = Standard error of the estimator).

Stage	Model	Bands	Regression equation	R^2	$R^2_{adj.}$	SE
Tillering	MLR-1	1	AGB = 1.638 - 19.715 ρ_{672}	0.334	0.332	0.348
n = 277	MLR-2	2	AGB = 1.051 - 16.182 ρ_{672} + 2.369 ρ_{1052}	0.498	0.494	0.303
	MLR-3	3	AGB = 1.189 + 12.021 ρ_{672} + 4.321 ρ_{1052} - 28.093 ρ_{696}	0.536	0.530	0.292
	MLR-4	4	AGB = 0.824 - 31.879 ρ_{672} + 70.423 ρ_{696} + 12.658 ρ_{814} - 60.408 ρ_{707}	0.641	0.636	0.257
Stem	MLR-1	1	AGB = -0.190 + 9.658 ρ_{780}	0.487	0.485	0.858
Elongation	MLR-2	2	AGB = 0.220 + 91.228 ρ_{780} - 86.560 ρ_{763}	0.633	0.629	0.728
n = 209	MLR-3	3	AGB = 0.518 + 72.709 ρ_{780} - 63.048 ρ_{763} -22.077 ρ_{1489}	0.679	0.674	0.682
	MLR-4	4	AGB = 1.277 + 26.058 ρ_{780} - 24.207 ρ_{763} - 66.429 ρ_{1489} + 30.298 ρ_{1662}	0.744	0.739	0.611
Booting	MLR-1	1	AGB = 1.374 + 8.697 ρ_{854}	0.443	0.441	1.180
n = 232	MLR-2	2	AGB = 1.772 + 17.572 ρ_{854} - 19.088 ρ_{729}	0.533	0.529	1.083
	MLR-3	3	AGB = 1.555 + 24.049 ρ_{854} - 14.718 ρ_{729} - 10.531 ρ_{1172}	0.545	0.539	1.071
	MLR-4	4	AGB = 1.147 + 28.131 ρ_{854} - 20.997 ρ_{729} - 12.945 ρ_{1172} + 69.257 ρ_{377}	0.560	0.552	1.056
Heading	MLR-1	1	AGB = 9.970 - 256.497 ρ_{380}	0.066	0.062	1.816
n = 297	MLR-2	2	AGB = 7.798 - 255.759 ρ_{380} + 5.190 ρ_{1083}	0.119	0.113	1.766
	MLR-3	3	AGB = 7.842 - 263.838 ρ_{380} + 20.485 ρ_{1083} - 16.632 ρ_{1003}	0.166	0.157	1.722
	MLR-4	4	AGB = 6.445 - 488.717 ρ_{380} + 26.101 ρ_{1083} - 23.102 ρ_{1003} + 349.618 ρ_{406}	0.203	0.192	1.686
All	MLR-1	1	AGB = -1.534 + 20.179 ρ_{936}	0.629	0.628	1.889
n = 1015	MLR-2	2	AGB = -0.111 + 29.231 ρ_{936} - 25.930 ρ_{1659}	0.745	0.745	1.565
	MLR-3	3	AGB = 0.137 + 46.188 ρ_{936} - 24.244 ρ_{1659} - 18.150 ρ_{762}	0.757	0.756	1.529
	MLR-4	4	AGB = 0.481 + 37.904 ρ_{936} - 30.875 v_{1659} - 27.087 ρ_{762} + 18.429 ρ_{1027}	0.771	0.770	1.485

mass variability. However, the results indicated that the best MLR model was dependent on the number of independent variables. A higher number of variables cause higher R^2 values, but the number of bands has a limit. Fig. 6 demonstrates the relationship between the band number and the performance of the MLR models at each stage. The relation is illustrated as a curve for each stage. The curves are characterised by four features: Linear rise, saturation, again linear rise and finally asymptotic trend. Despite the stepwise increasing of bands, the performance of the models showed an indication of overfitting (after 2–3 bands). iii) For this reason, the optimal number was set to four. The best MLR models are listed in Tab. 3 separately for each stage and across all stages.

Tab. 4: Calibration results versus validation results (NRI = normalized ratio index, SR = simple ratio, MLR = multiple linear regression).

Calibration dataset		(2007–2009)	Validation dataset			
Stage	R^2	Model $_{(\rho)}$	**RMSE**	**RE**	**R^2**	Stage
	0.56	NRI $_{(799,711)}$	0.58	54.8	0.70	
	0.58	SR $_{(822, 716)}$	0.57	53.9	0.69	
Tillering	0.30	MLR-1 $_{(672)}$	0.66	57.6	0.29	Tillering
n = 277	0.44	MLR-2 $_{(672, 1052)}$	0.61	53.0	0.55	n = 92
	0.47	MLR-3 $_{(672, 1052, 696)}$	0.56	53.0	0.62	
	0.56	MLR-4 $_{(672, 696, 814, 707)}$	0.47	44.5	0.82	
	0.76	NRI $_{(1678, 1575)}$	1.25	59.4	0.38	
	0.53	SR $_{(1760, 1325)}$	1.36	64.8	0.45	
Stem Elongation	0.49	MLR-1 $_{(780)}$	1.88	89.3	0.18	Stem Elongation
n = 209	0.63	MLR-2 $_{(780, 763)}$	1.28	60.8	0.31	n = 130
	0.68	MLR-3 $_{(780, 763, 1489)}$	1.15	54.8	0.51	
	0.74	MLR-4 $_{(780, 763, 1489, 1662)}$	1.16	55.1	0.42	
	0.54	NRI $_{(695, 515)}$	1.89	49.3	0.00	
	0.54	SR $_{(695, 513)}$	3.49	90.8	0.00	
Booting	0.44	MLR-1 $_{(854)}$	1.89	49.3	0.14	Booting
n = 232	0.53	MLR-2 $_{(854, 729)}$	2.07	53.8	0.06	n = 257
	0.54	MLR-3 $_{(854, 729, 1172)}$	1.98	49.7	0.12	
	0.56	MLR-4 $_{(854, 729, 1172, 377)}$	1.86	48.4	0.11	
	0.29	NRI $_{(800, 789)}$	2.73	51.3	0.19	
	0.22	SR $_{(800, 789)}$	2.76	51.9	0.19	
Heading	0.02	MLR-1 $_{(380)}$	3.12	58.6	0.01	Heading
n = 297	0.04	MLR-2 $_{(380, 1083)}$	3.12	58.6	0.01	n = 191
	0.05	MLR-3 $_{(380, 1083, 1003)}$	3.09	58.1	0.02	
	0.06	MLR-4 $_{(380, 1083, 1003, 406)}$	2.86	53.8	0.12	
	0.74	NRI $_{(713, 533)}$	2.86	76.0	0.42	
	0.76	SR $_{(713, 550)}$	2.76	77.9	0.70	
All	0.60	MLR-1 $_{(936)}$	2.57	72.7	0.48	All
n = 1015	0.72	MLR-2 $_{(936, 1659)}$	2.42	68.4	0.53	n = 670
	0.74	MLR-3 $_{(936, 1659, 762)}$	2.44	68.9	0.54	
	0.75	MLR-4 $_{(936, 1659, 762, 1027)}$	2.49	70.2	0.55	

The results indicate that regression equations and the significant bands vary between the phenological stages. The performance of the models was improved by adding stepwise an additional independent band. For example at stem elongation, the R^2 values increased from 0.48 (MLR-1) to 0.74 (MLR-4) and across all stages from 0.62 (MLR-1) to 0.77 (MLR-4). Due to the high sample number, all results are significant at $p < 0.0001$ except for the heading stage. It is striking that many of the bands are located in the NIR and SWIR domain, but only some in the VIS domain.

3.6 *Calibration against Validation*

The calibrated (SR-, NRI-, MLR-) models were validated by an independent dataset (Tab. 4). Generally, the models using 2–4 single bands are the most promising for estimating AGB. Only one band explained AGB variability the least. In the case of MLR, the models tended to overfit already when fitting with 2–3 bands. This caused a slight increase of the R^2 and the RMSE values, though more bands were used for modeling.

At the tillering stage, the top identified models all used RED (672 nm, 692 nm) and NIR bands (707 nm – 1052 nm), while at the stem elongation stage NIR bands (763 nm, 780 nm) and SWIR bands (1325 nm – 1760 nm) dominated, and across all stages GREEN bands (533 nm, 550 nm), NIR bands (713 nm – 1027 nm) and a SWIR band (1659 nm) were selected. In most cases, the validated MLR-models provided the best results with highest R^2 values ($R^2 = 0.82$ at the tillering stage, $R^2 = 0.51$ at the stem elongation stage). The performance of the models at the booting and heading stages was worse ($R^2 < 0.19$). In addition, the RMSE values increased till to 3.49 t/ha. These models are useless for regionalisation. Across all stages, the SR showed its best performance ($R^2 = 0.70$). The RMSE values are reasonable, but the RE shows relatively high values (RE > 40 %). This fact can be explained through the different management of the experimental fields (manual work by fieldworkers) and farmers' fields (mechanical work by tractors and airplanes) and the different plot size (small scale farm-

ing in experiments and large scale in farmers' fields). When the SR-, NRI-, and MLR-models were evaluated with data from farmers' fields, the R^2 values were significantly smaller (0.38–0.51 at the stem elongation stage and 0.42–0.70 across all stages). However, at the tillering stage, the R^2 values were significantly higher (0.62–0.82) than the calibration values.

4   Discussion and Conclusion

In comparison to reflectance-based estimation of AGB for wheat or other cereals, the estimation of rice AGB is linked with a lower relationship between reflectance and AGB resulting in a lower R^2 performance of the models. Single bands, optimised SR and NRI, as well as MLR-based methods were able to explain 80 % – 90 % of the biomass variability in wheat, e.g. Zhu et al. (2008), Bao et al. (2009), Koppe et al. (2010), but only 60 % – 80 % in rice, e.g. Patel et al. (1985), Shibayama & Akiyama (1989), Takahashi et al. (2000), Wang et al. (2008), and Bajwa et al. (2010).

In this study, the performance of the investigated indices SR and NRI ($R^2 = 0.75$) was in the range of published studies, while MLR performed better ($R^2 = 0.93$). The bands of NRI were similar as in the study of Stroppiana et al. (2009) for rice AGB across all stages. Their analysis indicated highly correlated AGB ($R^2 > 0.9$) in the RedEdge. In the case of MLR, the optimal bands in this investigation were comparable to those by Wang et al. (2008). They also set the optimal band number to four to estimate AGB of rice, and they detected several bands in the SWIR domain. There was a clear cluster of SWIR bands, especially at the stem elongation stage, when the rice AGB was highly correlated with LAI (Gnyp et al. 2012). These bands represent the maximum reflectance in the 1500 nm – 1800 nm domain and are sensitive to lignin, starch and protein (Kumar et al. 2003).

Furthermore, one key objective of our study was the transfer of the optimised SIs and newly developed MLR models, which were investigated from data collected in field experiments, to real practice: Farmers' rice fields under conventional management. In this study, the up-scaling from the experimental to the

farmers' field level was promising using 2–4 bands by SR, NRI and MLR at the tillering ($R^2 = 0.82$) and the stem elongation stage ($R^2 = 0.51$). Prosperous scaling approaches from plots to the regional level were demonstrated to estimate LAI (Lausch et al. 2012), plant diseases (Laudien & Bareth 2006), or AGB in wheat (Koppe et al. 2012). But also high resolution and multi-temporal TerraSAR-X images indicated a high potential ($R^2 = 0.80$) of estimating rice AGB, e.g. Koppe et al. (2013). However, these studies focused on SIs or radar backscatter to transfer the models.

Several problems occurred during upscaling in this study, e.g., RedEdge shift and model overfitting. Best performing bands changed at different growth stages due to an increase or decrease of canopy reflectance in diverse spectral regions. Probably, the shift of the RedEdge and changes in the chlorophyll concentration due to the different N-application or different management in experimental and farmers' fields caused problems in model transferability. Temporal changes in RedEdge and chlorophyll concentration are a known fact, e.g. Horler et al. (1983) and Fillela & Penuelas (1994). The overfitting occurred with 2–3 bands and reduced the model predictability by MLR. Therefore, more bands improved the statistical relation, but not the model transferability. Nevertheless, since MLR is widely used for AGB estimation, PLS could probably improve the results. Hansen & Schjoerring (2003) showed that PLS performed better in predicting AGB compared to SIs. In a study for AGB estimation of rice, Thakahashi et al. (2000) achieved a better fitting by MLR, but a worse predictability than by PLS. Their results are comparable to this study at the stem elongation stage. In addition, the AGB variability is also diverse at each stage. The highest variability in AGB was observed, especially at the stem elongation stage. Probably, the water of the paddy field, but also wet soil could partly have some impact in the models at the tillering and stem elongation stages, when the plant cover was low. Since the same rice cultivar was planted in the experimental as well as in the farmers' fields, it should have no influence on the models. The different management such as controlled conditions in experimental and uncontrolled ones in farmers' fields might

be a problem. Up-scaling from small experimental to larger farmers' fields often yielded lower model predictability, e.g. Li et al. (2010) and Psomas et al. (2011), like in this study at the stem elongation stage.

Several different calculations could have been carried out in this study to partially avoid overfitting with MLR. For example, prior studies have shown that PLS, support vector machine (SVM), principle component analysis (PCA) and neural network approaches can also partly help to avoid this problem. In addition, the comparison of estimation of fresh and dry AGB would be of great value, since several studies displayed a better predictability of fresh rice AGB, e.g. Yang & Chen (2004). Due to the changing of the reflectance characteristics in the different plant organs, the AGB estimation should be investigated in the different organs leaf, stem and head as well. Future studies should involve data from large fields for calibration and for validation, which should be independent of each other. Moreover, sensor fusion could improve the validation as well, as shown for the radar and hyperspectral data combination by Koppe et al. (2012). Better development or validation of reliable models could be also achieved by cross-validation and bootstrapping (Richter et al. 2012).

After several improvements, the models of this study, especially these with high predictability at the tillering and stem elongation stages, could be tested by EnMap or other sensors from the space. This study showed the high potential in estimating dry AGB by MLR with 3–4 independent bands, but also by SR and NRI. These bands could be easily tested and evaluated for a larger area by UAVs (unmanned aerial vehicles) carrying hyperspectral sensors or cameras, or by satellite-borne hyperspectral sensors such as EO-1 Hyperion and EnMap, or the airborne sensor HyMap.

Acknowledgements

References

AGRICON, 2013: www.agricon.de (4.5.2013).

ANDERSON, G.L. & HANSON, J.D., 1992: Evaluating hand-held radiometer derived vegetation indices for estimating above ground biomass. – Geocarto International **7** (1): 71–78.

BAJWA, S.G., MISHRA, A.R. & NORMAN, R.J., 2010: Canopy reflectance response to plant nitrogen accumulation in rice. – Precision Agriculture **11** (5): 488–506.

BAO, Y., GAO, W. & GAO, Z., 2009: Estimation of winter wheat biomass based on remote sensing data at various spatial and spectral resolutions. – Frontier of Earth Science in China **3** (1): 118–128.

CHO, M.A. & SKIDMORE, A.K., 2009: Hyperspectral predictors for monitoring biomass production in Mediterranean grasslands: Majella National Park, Italy. – International Journal of Remote Sensing **30** (2): 499–515.

FAGIERA, N.K., 2007: Yield physiology of rice. – Journal of Plant Nutrition **30** (6): 843–879.

FILLELA, I. & PENUELAS, J., 1994: The red edge position and shape as indicators of plant chlorophyll content, biomass and hydric status. – International Journal of Remote Sensing **15** (7): 1459–1470.

GEBBERS, R. & ADAMCHUK, V.I., 2010: Precision agriculture and food security. – Science **327** (12): 828–831.

GNYP, M.L., YAO, Y., YU, K., HUANG, S., AASEN, H., LENZ-WIEDEMANN, V.I.S., MIAO, Y. & BARETH, G., 2012: Hyperspectral analysis of rice phenological stages in Northeast China. – ISPRS Annals of the Photogrammetry, Remote Sensing and Spatial Information Science, Melbourne, Australia, Volume **I-7:** 77–82.

HABOUDANE, D., MILLER, J.R., PATTEY, E., ZARCO-TEJADA, P.J. & STRACHAN, I.B., 2004: Hyperspectral vegetation indices and novel algorithms for predicting green LAI of crop canopy: Modeling and validation in the context of precision agriculture. – Remote Sensing of Environment **90** (3): 337–352.

HANSEN, P.M. & SCHJOERRING, J.K., 2003: Reflectance measurement of canopy biomass and nitrogen status in wheat crops using normalized difference vegetation indices and partial least squares regression. – Remote Sensing of Environment **86** (4): 542–553.

HORLER, D.N.H., DOCKRAY, M. & BARBER, J., 1983: The red edge of plant leaf reflectance. – International Journal of Remote Sensing **4** (2): 273–288.

JORDAN, C.F., 1969: Derivation of leaf area index from quality of light on the forest floor. – Ecology **50:** 663–666.

KAUFMANN, H., SEGL, K., ITZEROTT, S., BACH, H., WAGNER, A., HILL, J., HEIM, B., OPPERMANN, K., HELDENS, W., STEIN, E., MÜLLER, A., VAN DER LINDEN, S., LEITAO, P.J. & HOSTERT, P., 2010: Hyperspectral algorithms – Report in the frame of EnMAP preparation activities. – Deutsches GeoForschungsZentrum GFZ **10** (8): 1–268.

KOPPE, W., LI, F., GNYP, M.L., MIAO, Y., JIA, L., CHEN, X., ZHANG, F. & BARETH, G., 2010: Evaluating multispectral and hyperspectral satellite remote sensing data for estimating winter wheat growth parameters at regional scale in North China Plain. – PFG – Photogrammmetrie, Fernerkundung, Geoinformation **2010** (3): 167–178.

KOPPE, W., GNYP, M.L., HENNIG, S.D., LI, F., MIAO, Y., CHEN, X., JIA, L. & BARETH, G., 2012: Multitemporal hyperspectral and radar remote sensing for estimating winter wheat biomass in the North China Plain. – PFG – Photogrammmetrie, Fernerkundung, Geoinformation **2012** (3): 281–298.

KOPPE, W., GNYP, M.L., HÜTT, C., YAO, Y., MIAO, Y., CHEN, X. & BARETH, G., 2013: Rice monitoring with multi-temporal and dual-polarimetric TerraSAR-X data. – International Journal of Applied Earth Observation and Geoinformation **21:** 568–576.

KUMAR, L., SCHMIDT, K., DURRY, S. & SKIDMORE, A., 2003: Imaging spectrometry and vegetation science. – VAN DER MEER, F.D. & DE JONG, S.M. (eds): Imaging Spectrometry, Dordrecht, The Netherlands.

Laudien, R. & Bareth, G., 2006: Multitemporal hyperspectral data analysis for regional detection of plant diseases by using a tractor- and an airborne-based spectrometer. – PFG – Photogrammetrie, Fernerkundung, Geoinformation **2006** (3): 217–227.

Lausch, A., Pause, M., Merbach, I., Gwillym-Margianto, S., Schulz, K., Zacharias, S. & Seppelt, R., 2012: Scale-specific hyperspectral remote sensing approach in environmental research. – PFG – Photogrammetrie, Fernerkundung, Geoinformation **2012** (5): 589–602.

Li, F., Miao, Y., Hennig, S.D., Gnyp, M.L., Chen, X., Jia, L. & Bareth, G., 2010: Evaluating hyperspectral vegetation indices for estimating nitrogen concentration of winter wheat at different growth stages. – Precision Agriculture **11** (4): 335–357.

Lu, D., 2006: The potential and challenge of remote sensing-based biomass estimation. – International Journal of Remote Sensing **27** (7): 1297–1328.

MATLAB, 2013: MathWorks Inc., Natick, MA, USA, www.mathwork.de (4.5.2013).

Milton, E.J., Schaepman, M.E., Anderson, K., Kneubühler, M. & Fox, N., 2009: Progress in field spectroscopy. – Remote Sensing of Environment **113** (1): 92–109.

Ortenberg, F., 2011: Hyperspectral sensor characteristics: airborne, spaceborne, hand-held, and truck-mounted; Integration of hyperspectral data with Lidar. – Thenkabail, P.S., Lyon, J.G. & Huete, A. (eds): Hyperspectral remote sensing of vegetation. Boca Raton, FL, USA.

Patel, N.K., Singh, P., Sahai, B. & Patel, M.S., 1985: Spectral response of rice crop and its relation to yield and yield attributes. – International Journal of Remote Sensing **6** (5): 657–664.

Psomas, A., Kneubühler, M., Huber, S., Itten, K. & Zimmermann, N.E., 2011: Hyperspectral remote sensing for estimating aboveground biomass and for exploring species richness patterns of grassland habitats. – International Journal of Remote Sensing **32** (24): 9007–9031.

Raun, W.R. & Johnson, G.V., 1999: Improving nitrogen use efficiency for cereal production. – Agronomy Journal **91** (3): 357–363.

Richardson, A.J., Everitt, J.H. & Gausman, H.W., 1983: Radiometric estimation of biomass and nitrogen content of Alicia Grass. – Remote Sensing of Environment **13** (2): 179–185.

Richter, K., Atzberger, C., Hank, T.B. & Mauser, W., 2012: Derivation of biophysical variables from Earth observation data: validation and statistical measures. – Journal of Applied Remote Sensing **6** (1): 179–185.

Rouse, J.W., Has, R.H., Schell, J.A. & Deering, D.W., 1974: Monitoring vegetation systems in the Great Plains with ERTS. – Third ERTS Symposium, NASA Sp-3511: 309–317.

Schwind, P., Müller, R., Palubinskas, G. & Storch, T., 2012: An in-depth simulation of EnMAP acquisition geometry. – ISPRS Journal of Photogrammetry and Remote Sensing **70** (1): 99–106.

Serrano, L., Filella, I. & Penuelas, J., 2000: Remote sensing of biomass and yield of winter wheat under different nitrogen supplies. – Crop Science **40** (3): 723–731.

Shibayama, M. & Munakata, K., 1986: A spectroradiometer for field use III: A comparison of some vegetation indices for predicting luxuriant paddy rice biomass. – Japanese Journal of Crop Science **55** (1): 47–52.

Shibayama, M. & Akiyama, K., 1989: Seasonal visible, near-infrared and mid-infrared spectra of rice canopies in relation to LAI and aboveground dry phytomass. – Remote Sensing of Environment **27** (2): 119–127.

Sims, D.A. & Gamon, J.A., 2002: Relationship between leaf pigment content and spectral reflectance across a wide range of species, leaf structure and development stages. – Remote Sensing of Environment **81** (2–3): 337–354.

Song, S., Gong, W., Zhu, B. & Huang, X., 2011: Wavelength selection and spectral discrimination for paddy rice with laboratory measurements of hyperspectral leaf reflectance. – ISPRS Journal of Photogrammetry and Remote Sensing **66** (5): 672–682.

SPSS, 2013: IBM SPSS Inc., Armonk, NY, USA, www-01.ibm.com/software/analytics/spss (4.5.2013).

Statistica, 2013: StatSoft, Tulsa, OK, USA, www.statsoft.com (4.5.2013).

Stroppiana, D., Boschetti, M., Brivio, P.A. & Bocchi, S., 2009: Plant nitrogen concentration in paddy rice from canopy hyperspectral radiometry. – Field Crops Research **111** (1–2): 119–129.

Takahashi, W., Nguyen-Cong, V., Kawaguchi, S., Minamiyama, M. & Ninomiya, S., 2000: Statistical models for prediction of dry weight and nitrogen accumulation based on visible and near-infrared hyper-spectral reflectance of rice canopies. – Plant Production Science **3** (4): 377–386.

Thenkabail, P.S., Smith, R.B. & Pauw, E.D., 2000: Hyperspectral vegetation indices and their relationship with agricultural crop characteristics. – Remote Sensing of Environment **71** (2): 152–182.

Wang, F., Huang, J. & Wang, X., 2008: Identification of optical hyperspectral bands for estimation of rice biophysical parameters. – Journal of Integrative Plant Biology **50** (3): 291–299.

YANG, C. & CHEN, R., 2004: Modeling rice growth with hyperspectral reflectance data. – Crop Science **44** (4): 1283–1290.

YU, K., LI, F., GNYP, M.L., MIAO, Y., BARETH, G. & CHEN, X., 2013: Remotely detecting canopy nitrogen concentration and uptake of paddy rice in Northeast China Plain. – ISPRS Journal of Photogrammetry and Remote Sensing **78:** 102–115.

ZHU, Y., YAO, X., TIAN, Y., LIU, X. & CAO, W., 2008: Analysis of common canopy vegetation indices for indicating leaf nitrogen accumulation wheat and rice. – International Journal of Applied Earth Observation and Geoinformation **10** (1): 1–10.

Address of the Authors:

MARTIN LEON GNYP, KANG YU, HELGE AASEN, Prof. Dr. GEORG BARETH, International Center for Agro-Informatics and Sustainable Development (www.icasd.org), Institute of Geography, GIS & RS Group, University of Cologne, D-50923 Köln, Tel.: +49-221-470-6551, Fax: +49-221-470-1638, e-mail: {mgnyp1}{kyu}{helge.aasen}{g.bareth}@uni-koeln.de

Ass. Prof. Dr. YUXIN MIAO, YINKUN YAO, SHANYU HUANG, International Center for Agro-Informatics and Sustainable Development (www.icasd.org), College of Resources and Environmental Sciences, China Agricultural University, 100094 Beijing, Tel.: +86-10-62732865, Fax: +86-10-62731016, e-mail: ymiao@cau.edu.cn, yyk719@163.com, shuang 331919@gmail. com